Anisotropic vortex lattice structures in the FeSe superconductor

Hsiang-Hsuan Hung,[1,*] Can-Li Song,[2] Xi Chen,[2] Xucun Ma,[3] Qi-kun Xue,[2] and Congjun Wu[1,4]
[1]*Department of Physics, University of California, San Diego, California 92093, USA*
[2]*State Key Laboratory for Low-Dimensional Quantum Physics, Department of Physics, Tsinghua University, Beijing 100084, China*
[3]*Institute of Physics, Chinese Academy of Sciences, Beijing 100190, China*
[4]*Center for Quantum Information, IIIS, Tsinghua University, Beijing, China*
(Received 28 September 2011; published 14 March 2012)

In the recent work by Song *et al.* [Science **332**, 1410 (2011)], the scanning tunneling spectroscopy experiment in the stoichiometric FeSe revealed evidence for nodal superconductivity and strong anisotropy. The nodal structure can be explained with the extended s-wave pairing structure with the mixture of the $s_{x^2+y^2}$ and $s_{x^2y^2}$ pairing symmetries. We calculate the anisotropic vortex structure by using the self-consistent Bogoliubov–de Gennes mean-field theory. In considering the absence of magnetic ordering in the FeSe at ambient pressure, orbital ordering is introduced, which breaks the C_4 lattice symmetry down to C_2, to explain the anisotropy in the vortex tunneling spectra.

DOI: 10.1103/PhysRevB.85.104510 PACS number(s): 74.20.Rp, 71.10.Fd, 74.20.Mn

I. INTRODUCTION

Since the first iron-based layered superconductor $La(O_{1-x}F_x)FeAs$ had been discovered,[1] the family of iron-based superconductors has made a huge impact in the condensed matter physics community. These novel materials exhibit similar phase diagrams compared to high-T_c cuprates. The parent compound LaOFeAs has an antiferromagnetic spin-density wave order,[2] and, upon doping, superconductivity appears. Although correlation effects are weaker in iron-based superconductors than those in high-T_c cuprates, novel features arise from the multiorbital degree of freedom. The orbital band structures play a fundamental role in determining the Fermi surface configurations and pairing structures.

Understanding pairing symmetries is one of the most important issues in the study of iron-based superconductors. Based on various experimental[3–5] and theoretical works,[6–10] the nodeless $s_{x^2y^2}$ wave pairing has been proposed. In momentum space, the Fermi surfaces of many iron-based superconductors consist of hole pockets around the Γ point, and electron pockets around the two M points. The signs of the pairing order parameters on electron and hole Fermi surfaces are opposite. The nodal lines of the gap function have no intersections with Fermi surfaces; thus, the $s_{x^2y^2}$ pairing is nodeless. In the itinerant picture, the Fermi surface nesting between the hole and the electron pockets facilitates the antiferromagnetic fluctuations which favor the $s_{x^2y^2}$ pairing.[11] In real space, an intuitive picture of the $s_{x^2y^2}$ wave pairing is just the next-nearest-neighbor (NNN) spin-singlet pairing with the s-wave symmetry.[6] Because the anion locations are above or below the centers of the iron-iron plaquettes, the NNN antiferromagnetic exchange J_2 is at the same order of the nearest-neighbor (NN) one, J_1. The NNN $s_{x^2y^2}$ wave pairing can be obtained from the decoupling of the J_2 term. On the other hand, various experimental results have shown signatures of nodal pairing structures.[12–14] In the framework of the s-wave pairing, nodal pairing can be achieved through the $s_{x^2+y^2}$ pairing.[15–17] The possibility for $s_{x^2+y^2}$ wave pairing in iron-based superconductors has also been shown in the functional renormalization group calculation.[18]

Another important aspect of the iron-based superconductors is the spontaneous anisotropy of both the lattice and the electronic degrees of freedom, which reduces the fourfold rotational symmetry to twofold. For example, LaOFeAs undergoes a structural orthorhombic distortion and a long-range spin-density wave (SDW) order at the wave vector $(\pi,0)$ or $(0,\pi)$.[2] A similar phenomenon was also detected in NdFeAsO by using polarized and unpolarized neutron-diffraction measurements.[19] One popular explanation of the nematicity is the coupling between lattice and the stripelike SDW order.[20,21] The SDW ordering has also been observed in the FeTe system but with a different ordering wave vector at $(\frac{\pi}{2},\frac{\pi}{2})$.[22,23]

Very recently, the experimental results of the FeSe superconductor reported by Song *et al.*[24] indicated a pronounced nodal pairing structure in scanning-tunneling spectroscopy. Strong electronic anisotropy is observed through the quasiparticle interference of the tunneling spectra at much higher energy than the superconducting gap. The low-energy tunneling spectra around the impurity and the vortex core also exhibit the anisotropy. The shapes of the vortex cores are significantly distorted along one lattice axis.

The anisotropy may arise from the structural transition from tetragonal to orthorhombic phase at 90 K. However, the typical orthorhombic lattice distortions in iron superconductors are on the order of 0.012 Å, which is about half a percent of the lattice constant and only leads to a tiny anisotropy in electronic structures.[24] In contrast, the anisotropic vortex cores and impurity tunneling spectra observed by Song *et al.* are clearly at the order of 1. Therefore, these anisotropies should be mainly attributed to the electronic origin. The antiferromagnetic long-range order in such a system may be a possible reason for the anisotropy. For example, it has been theoretically investigated that the stripelike SDW order can induce strong anisotropy in the quasiparticle interference of the STM tunneling spectroscopy.[25] However, no evidence of magnetic ordering has been found in FeSe at ambient pressure;[26] thus, this anisotropy should not be directly related to the long-range magnetic ordering.

On the other hand, orbital ordering is another possibility for nematicity in transition-metal oxides. For example, orbital ordering serves as a possible mechanism for the nematic metamagnetic states observed in $Sr_3Ru_2O_7$,[27,28] and its detection

through quasiparticle interference has been investigated.[29,30] Orbital ordering has also been suggested to lift the degeneracy between the d_{xz} and d_{yz} orbitals to explain the anisotropy in iron-based superconductors.

In this paper, we study the effect of orbital ordering on the vortex tunneling spectra in the FeSe superconductor. The rest of the paper is organized as follows. In Sec. II, a two-band model Hamiltonian and the relevant band parameters are introduced. The Bogoliubov–de Gennes mean-field formalism is described in Sec. III. In Sec. IV, we analyze the effects of orbital ordering on the tunneling spectra of mixed pairing of the NN $s_{x^2+y^2}$ wave and the NNN $s_{x^2y^2}$ wave in the homogeneous systems. In Sec. V, the effects of orbital ordering on the anisotropic vortex core tunneling spectra are investigated, which are in good agreement with experiments. Discussions and conclusions are given in Sec. VI.

II. MODEL HAMILTONIAN FOR THE BAND STRUCTURE

For simplicity, we use the two-band model involving the d_{xz} and d_{yz} orbital bands in a square lattice with each lattice site representing an iron atom, which was first proposed in Ref. 31. This is the minimal model describing the iron-based superconductors, which can also support orbital ordering. The tight-binding band Hamiltonian reads

$$H_0 = \sum_{\vec{r},\sigma} \left\{ H^{\rm NN}_{\parallel,\sigma} + H^{\rm NN}_{\perp,\sigma} + H^{\rm NNN}_{\sigma} - \mu n_{\vec{r}} \right\}, \tag{1}$$

where

$$\begin{aligned} H^{\rm NN}_{\parallel,\sigma} &= t^{\rm NN}_{\parallel}(d^{\dagger}_{xz,\sigma,\vec{r}} d_{xz,\sigma,\vec{r}+\hat{x}} + d^{\dagger}_{yz,\sigma,\vec{r}} d_{yz,\sigma,\vec{r}+\hat{y}}),\\ H^{\rm NN}_{\perp,\sigma} &= t^{\rm NN}_{\perp}(d^{\dagger}_{xz,\sigma,\vec{r}} d_{xz,\sigma,\vec{r}+\hat{y}} + d^{\dagger}_{yz,\sigma,\vec{r}} d_{yz,\sigma,\vec{r}+\hat{x}}),\\ H^{\rm NNN}_{\sigma} &= t^{\rm NNN}_{1}(d^{\dagger}_{xz,\sigma,\vec{r}} d_{xz,\sigma,\vec{r}\pm\hat{x}+\hat{y}} + d^{\dagger}_{yz,\sigma,\vec{r}} d_{yz,\sigma,\vec{r}\pm\hat{x}+\hat{y}})\\ &\quad + t^{\rm NNN}_{2}(d^{\dagger}_{xz,\sigma,\vec{r}} d_{yz,\sigma,\vec{r}+\hat{x}+\hat{y}} + d^{\dagger}_{yz,\sigma,\vec{r}} d_{xz,\sigma,\vec{r}+\hat{x}+\hat{y}})\\ &\quad + t^{\rm NNN}_{3}(d^{\dagger}_{xz,\sigma,\vec{r}} d_{yz,\sigma,\vec{r}-\hat{x}+\hat{y}} + d^{\dagger}_{yz,\sigma,\vec{r}} d_{xz,\sigma,\vec{r}-\hat{x}+\hat{y}}), \end{aligned} \tag{2}$$

where $d^{\dagger}_{a,\sigma,\vec{r}}$ denotes the creation operator for an electron with spin σ on the d_a orbital at site $\vec{r}$; d_a refers to d_{xz} and d_{yz} orbitals; $n_{\vec{r}} = n_{xz,\sigma,\vec{r}} + n_{yz,\sigma,\vec{r}}$, where $n_{a,\sigma,\vec{r}} = d^{\dagger}_{a,\sigma,\vec{r}} d_{a,\sigma,\vec{r}}$ denotes the particle number operator; μ is the chemical potential; $t^{\rm NN}_{\parallel}$ and $t^{\rm NN}_{\perp}$ denote the longitudinal σ bonding and transverse π bonding between NN sites, respectively; and the three NNN hoppings can be expressed in terms of the NNN σ and π bondings $t^{\rm NNN}_{\parallel}$ and $t^{\rm NNN}_{\perp}$, respectively, as $t^{\rm NNN}_1 = \frac{1}{2}(t^{\rm NNN}_{\parallel} + t^{\rm NNN}_{\perp})$, $t^{\rm NNN}_2 = \frac{1}{2}(t^{\rm NNN}_{\parallel} - t^{\rm NNN}_{\perp})$, and $t^{\rm NNN}_3 = \frac{1}{2}(-t^{\rm NNN}_{\parallel} + t^{\rm NNN}_{\perp})$. We depict the hopping schematic of the two-band tight-binding model Eq. (1) in Fig. 1.

By introducing the spinor $\Psi(\vec{k}) = [\psi_{xz,\sigma}(\vec{k}), \psi_{yz,\sigma}(\vec{k})]^T$ and performing the Fourier transformation, the Hamiltonian in momentum space becomes

$$H_0 = \sum_{\vec{k}} \Psi^{\dagger}_{a,\sigma}(\vec{k})\{H_{ab}(\vec{k}) + \varepsilon(\vec{k}) - \mu\delta_{ab}\}\Psi_{b,\sigma}(\vec{k}), \tag{3}$$

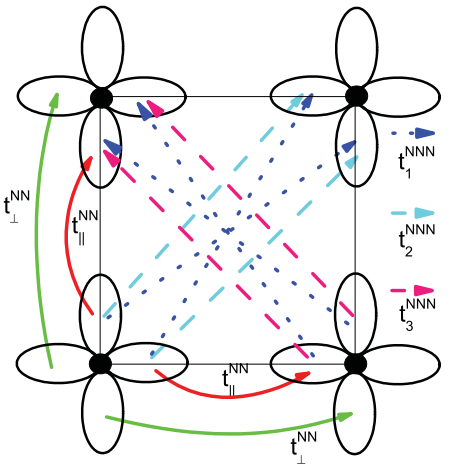

FIG. 1. (Color online) The hopping schematic of the two-band tight-binding model Eq. (1) in a unit cell. Each solid black circle represents an Fe atom. The solid arrows denote NN longitudinal σ-bonding (red) and transverse π-bonding (green) hoppings, respectively. The NNN intraorbital hoppings $t^{\rm NNN}_1$ are indicated by blue dotted arrows along the $\pm\hat{x} + \hat{y}$ directions. On the other hand, the NNN interorbital hoppings, $t^{\rm NNN}_2$ and $t^{\rm NNN}_3$, along the $\hat{x} + \hat{y}$ and $-\hat{x} + \hat{y}$ directions, respectively, are indicated by dashed cyan and pink arrows.

where a,b refer to the band index; the matrix kernel $H_{ab}(\vec{k})$ is written as

$$\begin{pmatrix} 2t^{\rm NN}_{\parallel}\cos k_x + 2t^{\rm NN}_{\perp}\cos k_y & 4t^{\rm NNN}_3 \sin k_x \sin k_y \\ \text{H.c.} & 2t^{\rm NN}_{\parallel}\cos k_y + 2t^{\rm NN}_{\perp}\cos k_x \end{pmatrix},$$

and $\varepsilon(\vec{k}) = 2\cos k_x \cos k_y (t^{\rm NNN}_{\parallel} + t^{\rm NNN}_{\perp})$. This two-orbital model has also been used to study impurity resonance states,[32,33] vortex core states,[34,35] and quasiparticle scattering inference.[36]

To fit the Fermi surface obtained from the local-density approximation calculations,[21] we use the parameter values below in the following discussions as

$$t^{\rm NN}_{\parallel} = 0.8, t^{\rm NN}_{\perp} = -1.4, t^{\rm NNN}_{\perp} = 1.8, t^{\rm NNN}_{\parallel} = 0, \tag{4}$$

all of which are in units of $t = 1$, which is roughly at an energy scale around 100 meV. This set of hopping integrals shows a similar band structure, as the one Raghu *et al.* used. The bandwidth is about 14. In the following discussion, we use $\mu = 1.15$, which corresponds to slightly hole-doped regimes. The unfolded Brillouin zone (UBZ) embraces a hole surface around the Γ point [$\vec{k} = (0,0)$], four hole pockets around the X point [$\vec{k} = (\pm\pi, \pm\pi)$] and four electron pockets around the M point [$\vec{k} = (0, \pm\pi)$ or $(\pm\pi, 0)$].[11,37]

Our main purpose is to study the anisotropy effects in FeSe due to the orbital ordering. Orbital ordering has been proposed in iron-based superconductors in previous studies.[38–43] Such an ordering may arise from the interplay between orbital, lattice, and magnetic degrees of freedom in iron superconductors. In this paper, we are not interested in the microscopic mechanism of spontaneous orbital ordering, but rather assume its existence to explain the vortex tunneling spectra observed in Ref. 24. According to the experimental data,[24] strong anisotropy has already been observed at least at an energy scale of 10 meV, which is much larger than the pairing gap value around

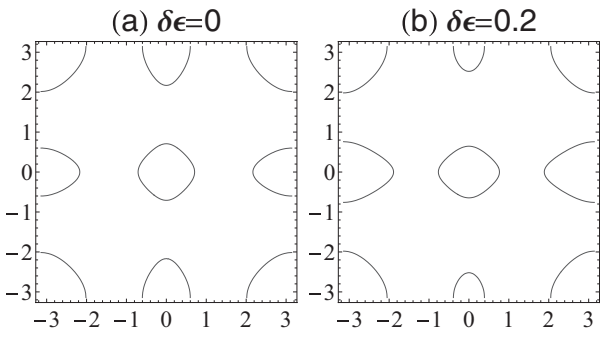

FIG. 2. (Color online) Fermi surfaces in the UBZ for (a) $\delta\varepsilon = 0$ and (b) $\delta\varepsilon = 0.2$. The horizontal and vertical axes denote k_x and k_y, respectively. The parameter values used are $t_{\parallel}^{\mathrm{NN}} = 0.8$, $t_{\perp}^{\mathrm{NN}} = -1.4$, $t_{\perp}^{\mathrm{NNN}} = 1.8$, $t_{\parallel}^{\mathrm{NNN}} = 0$, and $\mu = 1.15$. Anisotropic hole and electron pockets are shown in (b) at the Γ and M points, respectively.

2 meV. Thus, when studying superconductivity, we neglect the fluctuations of the orbital ordering but treat it as an external anisotropy. For this purpose, we add an extra anisotropy term into the band structure Eq. (1) as

$$H_{\mathrm{orb}} = \delta\varepsilon \sum_{\vec{r},\sigma} (d^{\dagger}_{xz,\sigma,\vec{r}} d_{xz,\sigma,\vec{r}} - d^{\dagger}_{yz,\sigma,\vec{r}} d_{yz,\sigma,\vec{r}}), \tag{5}$$

which makes the d_{xz} orbital energy higher than that of d_{yz}. For comparison, the Fermi surfaces without and with the anisotropy term Eq. (5) are depicted in Figs. 2(a) and 2(b), respectively. In Fig. 2(b), with the orbital term, the distortion of the electron and hole pockets in the x and y directions of the Fermi surfaces appears such that the anisotropy is derived in the iron-based superconductors.

III. THE BOGOLIUBOV–DE GENNES FORMALISM

In this section, we present the self-consistent Bogoliubov–de Gennes (BdG) formalism based on the band structure described in Sec. II. In principle, for this multiorbital system, the general pairing structure should contain a matrix structure involving both the intra- and interorbital pairings. Here for simplicity, we only keep the intraorbital pairing, which is sufficient to describe the anisotropy observed in the experiment by Song *et al.*[24]

The pairing interactions including the NN and NNN pairing are defined as

$$H_{\mathrm{int}} = -\frac{g_1}{2} \sum_{\langle \vec{r},\vec{r}' \rangle} \sum_{a} \hat{\Delta}^{\dagger}_{a}(\vec{r},\vec{r}') \hat{\Delta}_{a}(\vec{r},\vec{r}') - \frac{g_2}{2} \sum_{\langle\langle \vec{r},\vec{r}' \rangle\rangle} \sum_{a} \hat{\Delta}^{\dagger}_{a}(\vec{r},\vec{r}') \hat{\Delta}_{a}(\vec{r},\vec{r}'), \tag{6}$$

where a is the orbital index taking values of d_{xz} and d_{yz}; $\langle \vec{r},\vec{r}' \rangle$ represents the NN bonds and $\langle\langle \vec{r},\vec{r}' \rangle\rangle$ represents the NNN bonds; $g_{1,2}$ denotes the pairing interaction strengths along the NN and NNN bonds; and $\hat{\Delta}_a(\vec{r},\vec{r}')$ describes the spin singlet intraorbital pairing operator across the bond defined as

$$\hat{\Delta}_a(\vec{r},\vec{r}') = d_{a,\downarrow,\vec{r}} d_{a,\uparrow,\vec{r}'} - d_{a,\uparrow,\vec{r}} d_{a,\downarrow,\vec{r}'}. \tag{7}$$

where $\vec{r}' = \vec{r} + \vec{\delta}$. For the $s_{x^2+y^2}$ pairing along the NN bonds, $\vec{\delta} = a\hat{x}(\hat{y})$, whereas for the $s_{x^2y^2}$ pairing along the NNN bonds, $\vec{\delta} = \pm a(\hat{x} + \hat{y})$, where a is the Fe-Fe bond length, defined as the lattice constant. In the square lattice, these two pairings belong to the same symmetry class; thus, they naturally coexist. After the mean-field decomposition, the Hamiltonian becomes

$$H_{\mathrm{MF}} = H_0 - \frac{g_1}{2} \sum_{\langle \vec{r},\vec{r}' \rangle} \sum_{a} \Delta^{*}_{a}(\vec{r},\vec{r}') \hat{\Delta}_{a}(\vec{r},\vec{r}') - \frac{g_2}{2} \sum_{\langle\langle \vec{r},\vec{r}' \rangle\rangle} \sum_{a} \Delta^{*}_{a}(\vec{r},\vec{r}') \hat{\Delta}_{a}(\vec{r},\vec{r}') + \mathrm{H.c.}, \tag{8}$$

where $\Delta^{*}_{a}(\vec{r},\vec{r}') = \langle \hat{\Delta}^{\dagger}_{a}(\vec{r},\vec{r}') \rangle$ is the pairing order parameter and $\langle \cdots \rangle$ denotes the expectation value over the ground state.

The mean-field BdG Hamiltonian Eq. (8) can be diagonalized through the transformation as

$$\begin{pmatrix} c_{a,\uparrow}(\vec{r}) \\ c^{\dagger}_{a,\downarrow}(\vec{r}) \end{pmatrix} = \sum_{n} \begin{pmatrix} u_{a,n}(\vec{r}) & -v^{*}_{a,n}(\vec{r}) \\ v_{a,n}(\vec{r}) & u^{*}_{a,n}(\vec{r}) \end{pmatrix} \begin{pmatrix} \gamma_{a,n} \\ \gamma^{\dagger}_{a,n} \end{pmatrix}. \tag{9}$$

The eigenvectors associated with E_n of the above BdG equations are $(u_{a,n}(\vec{r}), v_{a,n}(\vec{r}))^T$ and the pairing order parameters can be further obtained self-consistently as

$$\Delta_a(\vec{r},\vec{r}') = \sum_{n} (u_n(\vec{r}) v^{*}_{n}(\vec{r}') + u_n(\vec{r}') v^{*}_{n}(\vec{r})) \tanh \frac{bE_n}{2}, \tag{10}$$

where $b = 1/k_B T$. After the wave functions are obtained self-consistently, the local density of states (LDOS), which is proportional to the conductance (dI/dV) in the scanning tunneling microscopy, can be further measured by

$$\rho(\vec{r},E) = \sum_{n,a} \{ |u_{a,n}(\vec{r})|^2 L(E - E_n) + |v_{a,n}(\vec{r})|^2 L(E + E_n) \}, \tag{11}$$

where $L(x)$ is the Lorentzian as $L(x) = \gamma/[\pi(x^2 + \gamma^2)]$ and γ are the energy-broadening parameters, usually set around 1×10^{-2}.

When we study the vortex lattice structure problem, the single-particle Hamiltonian Eq. (1) is modified by the magnetic vector potential as

$$H'_0 = \sum_{\vec{r}_i,\vec{r}_j,\sigma,a,b} t_{i,j;a,b} e^{i\frac{\pi}{\Phi_0}\int_{\vec{r}_j}^{\vec{r}_i} \vec{A}(\vec{r})\cdot d\vec{r}} d^{\dagger}_{a,\sigma,\vec{r}_i} d_{b,\sigma,\vec{r}_j}, \tag{12}$$

where $\Phi_0 = hc/2e$ is the quantized flux; a,b denote orbital indices and σ denotes the spin index; and $t_{i,j;a,b}$ represents $t_{\parallel}^{\mathrm{NN}}$, $t_{\perp}^{\mathrm{NN}}$, or $t_{1,2,3}^{\mathrm{NNN}}$, depending on the corresponding bonds and orbitals. The vector potential $\vec{A}(\vec{r})$ is chosen as the Landau gauge by $(A_x, A_y) = (0, Bx)$.

Due to the magnetic translational symmetry, we can apply the magnetic periodic boundary conditions to form Abrikosov vortex lattices. Each magnetic unit cell carries a magnetic flux of $2\Phi_0$, so each magnetic unit cell contains two vortices. We choose the size of the magnetic unit cell $pa \times qa$ with $p = 2q$, and the number of unit cells $N_x \times N_y$ with $N_y = 2N_x$. The corresponding magnetic field is $B = 2\Phi_0/pqa^2 = \Phi_0/(qa)^2$. In the Abrikosov vortex lattice, the translation vector is written as $\vec{\mathrm{V}} = (\mathrm{X}pa, \mathrm{Y}qa)$, where $\mathrm{X} = 0, \ldots, N_x - 1$ and $\mathrm{Y} = 0, \ldots, N_y - 1$ are integers. The coordinate of an arbitrary lattice site can be expressed as $\vec{R} = \vec{r} + \vec{\mathrm{V}}$, where $\vec{r} = (xa, ya)$ denotes the coordinate of the lattice site within a magnetic unit cell (i.e., $1 \leqslant x \leqslant p$ and $1 \leqslant y \leqslant q$).

Under the magnetic periodic boundary conditions, the eigenvectors of the BdG Eqs. (9) satisfy a periodic structure written as

$$\begin{pmatrix} u_{a,n}(\vec{r}+pa\hat{x}) \\ v_{a,n}(\vec{r}+pa\hat{x}) \end{pmatrix} = e^{iK_x} \begin{pmatrix} e^{2\pi i \frac{y}{q}} u_{a,n}(\vec{r}) \\ e^{-2\pi i \frac{y}{q}} v_{a,n}(\vec{r}) \end{pmatrix},$$
$$\begin{pmatrix} u_{a,n}(\vec{r}+qa\hat{y}) \\ v_{a,n}(\vec{r}+qa\hat{y}) \end{pmatrix} = e^{iK_y} \begin{pmatrix} u_{a,n}(\vec{r}) \\ v_{a,n}(\vec{r}) \end{pmatrix}. \quad (13)$$

Here $K_x = \frac{2\pi \mathrm{X}}{N_x}$ and $K_y = \frac{2\pi \mathrm{Y}}{N_y}$ represent the magnetic Bloch wave vector on the x and y components.[44] With the relation, we can simulate vortex lattices with sizes of $(N_x pa) \times (N_y qa)$ but reduce the computational effort by diagonalizing $N_x N_y$ Hamiltonian matrices with dimensions of $4pq$ rather than directly diagonalizing a $4N_x N_y pq$ Hamiltonian matrix.

IV. THE NODAL VERSUS NODELESS PAIRINGS

In this section, we investigate the behavior of the superconducting gaps in the homogeneous system. Due to the translation symmetry, the pairing order parameters are spatially uniform, and we define $\Delta_a(\vec{\delta}) = \Delta_a(\vec{r}, \vec{r}+\vec{\delta})$, where $a = d_{xz}, d_{yz}$. We start with the case in the absence of orbital ordering, i.e., $\delta\varepsilon = 0$. Due to the fourfold rotational symmetry, not all of the pairing order parameters are independent. For the NN bond pairing, we have $\Delta_{xz}(\hat{x}) = \Delta_{yz}(\hat{y})$ and $\Delta_{xz}(\hat{y}) = \Delta_{yz}(\hat{x})$ due to the s-wave symmetry. As for the NNN bonding, a similar analysis yields the relations $\Delta_{xz}(\hat{x}+\hat{y}) = \Delta_{yz}(-\hat{x}+\hat{y})$ and $\Delta_{xz}(\hat{x}-\hat{y}) = \Delta_{yz}(\hat{x}+\hat{y})$.

Due to the multiorbital structure, generally speaking, the pairing order parameters have the matrix structure; thus, the analysis of the pairing symmetry is slightly complicated. However, before the detailed calculation, we perform a simplified qualitative analysis by considering the trace of the pairing matrix, defined as

$$\Delta(\vec{\delta}) = \tfrac{1}{2}(\Delta_{xz}(\vec{\delta}) + \Delta_{yz}(\vec{\delta})) \quad (14)$$

for both of the NN and NNN bonds. These quantities play a major role in determining the pairing symmetry. The angular form factor of the Fourier transform of the NN s-wave pairing is $\Delta_{s_{x^2+y^2}}(k_x,k_y) \propto \cos k_x + \cos k_y$, and that of the NNN s-wave pairing is $\Delta_{s_{x^2y^2}}(k_x,k_y) \propto \cos k_x \cos k_y$. Naturally $\Delta_{s_{x^2+y^2}}$ and $\Delta_{x^2y^2}$ have the same phase. Otherwise there would be a large energy cost corresponding to the phase twist in a small length scale of lattice constant. The nodal lines of $\Delta_{s_{x^2+y^2}}$ have intersections with the electron pockets, whereas the nodal lines of $\Delta_{x^2y^2}$ do not have intersections with Fermi surfaces. Generally speaking, the NN and NNN s-wave pairings are mixed due to the same symmetry representation with the lattice group as

$$\Delta_{s_\pm}(k_x,k_y) = \Delta_1(\cos k_x + \cos k_y) + \Delta_2 \cos k_x \cos k_y. \quad (15)$$

It is well known that the gap function is nodal for the NN s-wave pairing, while it is nodeless for the NNN s-wave pairing. However, they can mix together. Recently this aspect was supported by a variational Monte Carlo calculation,[45] where the authors discovered that the $s_{x^2y^2}$-wave and $s_{x^2+y^2}$-wave states are energetically comparable. Our BdG calculations show that, even for the case of $g_2 \neq 0$ and $g_1 = 0$, the s-wave NN pairing is still induced by the g_2 term, and vice versa for the s-wave NNN pairing, showing that they can naturally coexist.

For the coexistence of the NN and NNN s-wave pairing, the pairing gap function can be either nodal or nodeless. For the pure NNN s-wave pairing, the nodal lines of the $\Delta_{x^2y^2}$ are $k_{x,y} = \pm\frac{\pi}{2}$, which have no intersections with any of the hole and electron pockets; thus, the pairing is nodeless. For the pure NN s-wave pairing, the nodal lines form a diamond box with four vertices at the M points $(\pm\pi,0)$ and $(0,\pm\pi)$, which intersects both electron pockets; thus, the pairing is nodal. When the NN and NNN s-wave pairings coexist, if the NN $s_{x^2+y^2}$-wave pairing is dominant, the nodal lines of the pairing function are illustrated in Fig. S6(a) of Ref. 46. The original diamond nodal box is deformed by pushing the four vertices away from the M points in the direction of the Γ point. If the deformation is small, the deformed diamond still intersects with the electron pockets, and thus the pairing remains nodal. Upon increasing the strength of the NNN pairing, the deformation is enlarged and the intersections disappear. Thus, the pairing is nodeless.

Figure 3 reveals the density of states (DOS) versus tunneling voltage for the mixed s-wave pairing state. The red open squares are obtained using stronger NNN pairing strength [i.e., $g_1 = 0.8$ and $g_2 = 1.2$ in Eq. (8)], providing gapful behavior which is similar to the pure $s_{x^2y^2}$-wave state. In this case, $\Delta_{xz}(\hat{x}) = \Delta_{yz}(\hat{y}) = 0.068$, $\Delta_{xz}(\hat{y}) = \Delta_{yz}(\hat{x}) = -0.077$, and $\Delta_{xz,yz}(\pm\hat{x} \pm \hat{y}) = 0.085$, showing stronger NNN $s_{x^2y^2}$-wave pairing than NN $s_{x^2+y^2}$-wave pairing. On the other hand, the black solid line (using $g_1 = 1.2$ and $g_2 = 0.4$) indicates a gapless V shape, similar to the pure $s_{x^2+y^2}$-wave state. Contrary to the former case, the NN pairing order parameters $\Delta_{xz}(\hat{x}) = \Delta_{yz}(\hat{y}) = 0.071$, $\Delta_{xz}(\hat{y}) = \Delta_{yz}(\hat{x}) = -0.059$ are larger than the NNN $s_{x^2y^2}$-wave ones $\Delta_{xz,yz}(\pm\hat{x} \pm \hat{y}) = 0.057$. This reveals that the competition between the gapful and gapless modes can be adjusted by tuning the ratios between NNN and NN pairing interactions.

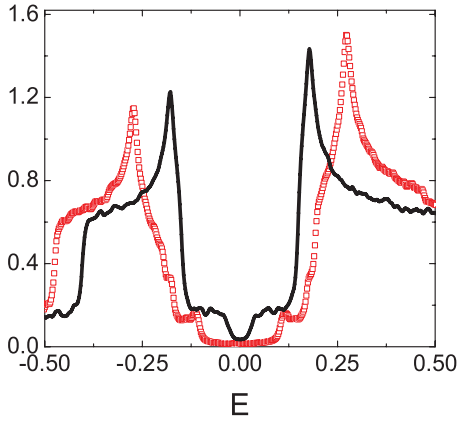

FIG. 3. (Color online) DOS vs tunneling bias E for the mixed s-wave pairing states at zero temperature. The red open squares with the parameter depict nodeless pairing with the dominant NNN pairing, and the black solid line depicts nodal pairing with the dominant NN pairing. The parameter values are $(g_1 = 0.8, g_2 = 1.2)$ for the nodeless case and $(g_1 = 1.2, g_2 = 0.4)$ for the nodal case, respectively.

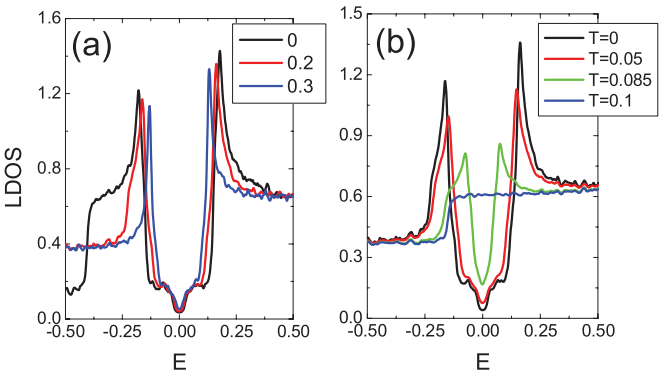

FIG. 4. (Color online) (a) DOS vs tunneling voltage E for extended $s_{\pm}$ wave without orbital anisotropy ($\delta\varepsilon = 0$) and with orbital anisotropy ($\delta\varepsilon = 0.2, 0.3$). Other parameter values are ($g_1 = 1.2, g_2 = 0.4$). At $\delta\varepsilon = 0$ the coherent peaks are around $E = \pm 0.18$ and upon increasing $\delta\varepsilon = 0$ the locations of the coherent peaks only slightly move toward zero energy. (b) The temperature dependence of the DOS vs E for the extended $s_{\pm}$ wave with orbital anisotropy $\delta\varepsilon = 0.2$ and the same parameters of $g_{1,2}$ as in (a). At $T = 0$, the coherent peaks are located at $E = \pm 0.165$.

The main goal of our paper is to determine the effect from orbital ordering which is mimicked by Eq. (5). With the anisotropy, the pairing structure changes from Eq. (15) to the following:

$$\Delta_{s_{\pm}}(k_x, k_y) = \Delta_1(\cos k_x + \lambda \cos k_y) + \Delta_2 \cos k_x \cos k_y, \quad (16)$$

where λ is determined by the anisotropy. The anisotropic nodal curve still intersects the electron pockets, as illustrated in Fig. S6(b) in Ref. 46, and thus the superconducting gap functions remain nodal. The calculated DOS versus energy patterns are plotted in Fig. 4(a) with the parameter values specified in the figure caption. Upon finite $\delta\varepsilon$, the pairing order parameters become anisotropic. For example, at $\delta\varepsilon = 0.2$, we have

$$\begin{aligned} \Delta_{xz}(\hat{x}) &= 0.059, \quad \Delta_{yz}(\hat{y}) = 0.070, \\ \Delta_{xz}(\hat{y}) &= -0.050, \quad \Delta_{yz}(\hat{x}) = -0.054, \\ \Delta_{xz}(\hat{x}+\hat{y}) &= \Delta_{xz}(-\hat{x}+\hat{y}) = 0.0503, \\ \Delta_{yz}(\hat{x}+\hat{y}) &= \Delta_{yz}(-\hat{x}+\hat{y}) = 0.0505, \end{aligned} \quad (17)$$

and the gapless gap function and the V-shaped spectra remain in the moderate anisotropy from orbital ordering.

We also check the temperature dependence of the DOS with the orbital ordering as presented in Fig. 4(b) with same parameter values of $g_{1,2}$ as in Fig. 4(a). With orbital anisotropy $\delta\varepsilon = 0.2$, the coherence peaks at zero temperature are approximately $\Delta_{\rm ch} \approx 0.165$. At low finite temperatures, say $T = 0.05 \approx 0.3\Delta_{\rm ch}$, the V-shaped DOS is still discernible. However, upon increasing temperatures the V-shaped LDOS patterns smear and eventually the coherent peaks disappear at $T = 0.1 \approx 0.6\Delta_{\rm ch}$. In this case the system turns into the normal state. This feature is qualitatively consistent with the experimental observation of the differential conductance spectra on FeSe in Ref. 24.

V. THE VORTEX STRUCTURE

In this section, we study the vortex tunneling spectra for the extended $s_{\pm}$-wave state. The size of the magnetic unit cell is chosen as $pa \times qa = 20a \times 40a$, which contains two vortices. The external magnetic field $B = 2\Phi_0/pqa^2$. The number of magnetic unit cells shown below is taken using $N_x \times N_y = 20 \times 10$, which is equivalent to the system size of $400a \times 400a$. The BdG equations are solved self-consistently with the tight-binding model Eq. (12) plus the mean-field interaction Eq. (6). The vortex configurations are investigated for both cases with and without orbital ordering in Secs. V A and V B, respectively. The interaction parameters are $g_1 = 1.2$ and $g_2 = 0.4$, and the temperature is fixed at zero.

A. Vortex structure in the absence of orbital ordering

We start with the vortex configuration without orbital ordering. The NN $s_{x^2+y^2}$-wave and NNN $s_{x^2y^2}$-wave pairing

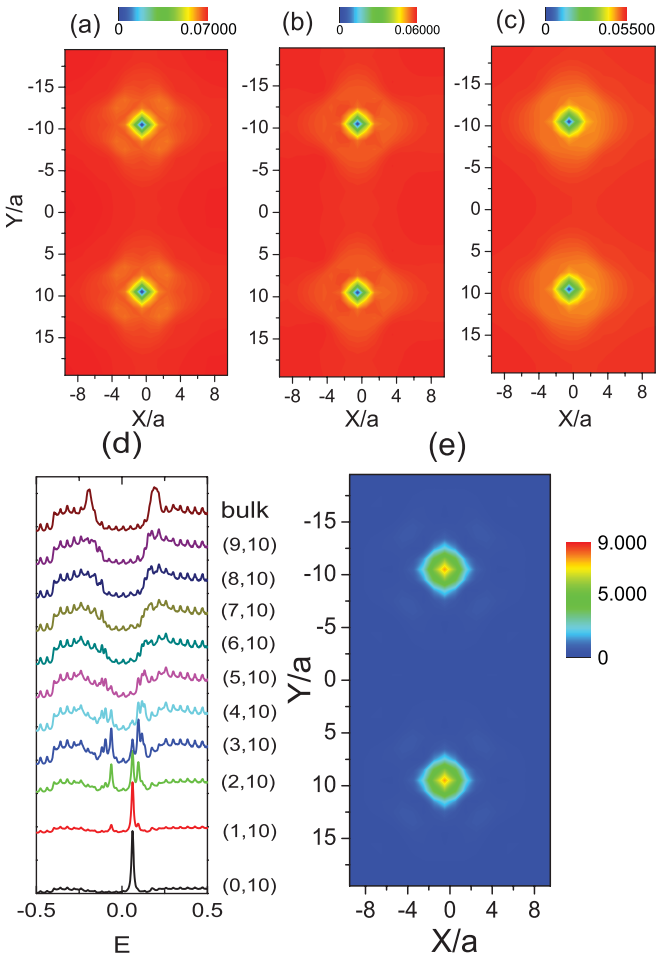

FIG. 5. (Color online) The vortex structure for the mixed NN $s_{x^2+y^2}$-wave and NNN $s_{x^2y^2}$-wave pairing without orbital ordering. Spatial distribution of the (a) longitudinal and (b) transverse NN pairings $\Delta_L^{\rm NN}(\vec{r})$ and $\Delta_T^{\rm NN}(\vec{r})$, respectively. (c) The NNN s-wave pairing order parameters $\Delta^{\rm NNN}(\vec{r})$. (d) LDOS vs E at different locations from the vortex core [at $\vec{r} = (0, 10a)$] to outside along the x axis. The distances of each site from the vortex core take the step of one lattice constant. (e) The spatial LDOS distribution at the energy of the vortex core resonance peak $E_{\rm re} \approx 0.062$.

order parameters in real space are defined as follows. We define the longitudinal and transverse NN s-wave pairings as

$$\begin{aligned}\Delta_L^{\mathrm{NN}}(\vec{r}) &= \tfrac{1}{4}\{\Delta_{xz}(\vec{r},\vec{r}+a\hat{x})+\Delta_{xz}(\vec{r},\vec{r}-a\hat{x})\\ &\quad+\Delta_{yz}(\vec{r},\vec{r}+a\hat{y})+\Delta_{yz}(\vec{r},\vec{r}-a\hat{y})\},\\ \Delta_T^{\mathrm{NN}}(\vec{r}) &= \tfrac{1}{4}\{\Delta_{yz}(\vec{r},\vec{r}+a\hat{x})+\Delta_{yz}(\vec{r},\vec{r}-a\hat{x})\\ &\quad+\Delta_{xz}(\vec{r},\vec{r}+a\hat{y})+\Delta_{xz}(\vec{r},\vec{r}-a\hat{y})\}.\end{aligned} \tag{18}$$

For the NNN pairing related to site $\vec{r}$, we define

$$\Delta^{\mathrm{NNN}}(\vec{r}) = \frac{1}{8}\sum_{a=xz,yz;\vec{\delta}=\pm\hat{x}\pm\hat{y}} \Delta_a(\vec{r},\vec{r}+\vec{\delta}). \tag{19}$$

The pure NN $s_{x^2+y^2}$-wave vortex states were recently investigated to describe the competition between the superconductivity and SDW in the hole-doped materials, $Ba_{1-x}K_xFe_2As_2$.[47] A similar calculation for the pure NNN $s_{x^2y^2}$ wave with SDW has been used to study $BaFe_{1-x}Co_xAs_2$ (Ref. 34) and the FeAs stoichiometric compounds.[35] In our case, these two s-wave pairing order parameters mix together.

The real space profiles of the longitudinal and transverse NN s-wave pairings $\Delta_L^{\mathrm{NN}}(\vec{r})$ and $\Delta_T^{\mathrm{NN}}(\vec{r})$ are depicted in Figs. 5(a) and 5(b), respectively. The vortex cores are located at $\vec{r} = (0, \pm 10a)$, where the pairing order parameters are suppressed. Both of them exhibit the C_4 symmetry. The NNN s-wave pairing order parameters are depicted in Fig. 5(c) and the vortices are diamond-shaped with the C_4 rotational symmetry. Note that the maximum magnitudes of the NNN $s_{x^2y^2}$-wave pairing order parameters are smaller than those of NN longitudinal and transverse $s_{x^2+y^2}$-wave pairing order parameters, due to the stronger NN pairing strength ($g_1 = 1.2$ and $g_2 = 0.4$). The coherence length can be estimated as $\xi \approx 4a \sim 5a$ from the spatial distributions of order parameters.

The relations of LDOS versus the tunneling energy E are presented in Fig. 5(d) at different locations from the vortex core to outside along the x axis. The LDOS pattern along the y axis is the same as Fig. 5(d) due to C_4 symmetry. Note that there exist fine oscillations in the LDOS pattern. This fine oscillation structure may come from the Landau oscillation, in

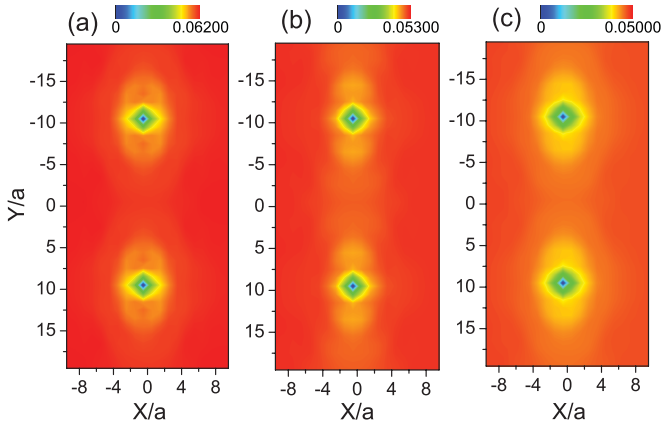

FIG. 6. (Color online) The spatial distributions of the s-wave pairing order parameters with the orbital anisotropy $\varepsilon = 0.2$. (a) The longitudinal NN pairing $\Delta_L^{\mathrm{NN}}(\vec{r})$, (b) the transverse NN pairing $\Delta_T^{\mathrm{NN}}(\vec{r})$, and (c) the NNN $s_{x^2y^2}$-wave pairing order parameters $\Delta^{\mathrm{NNN}}(\vec{r})$. All of them show anisotropy.

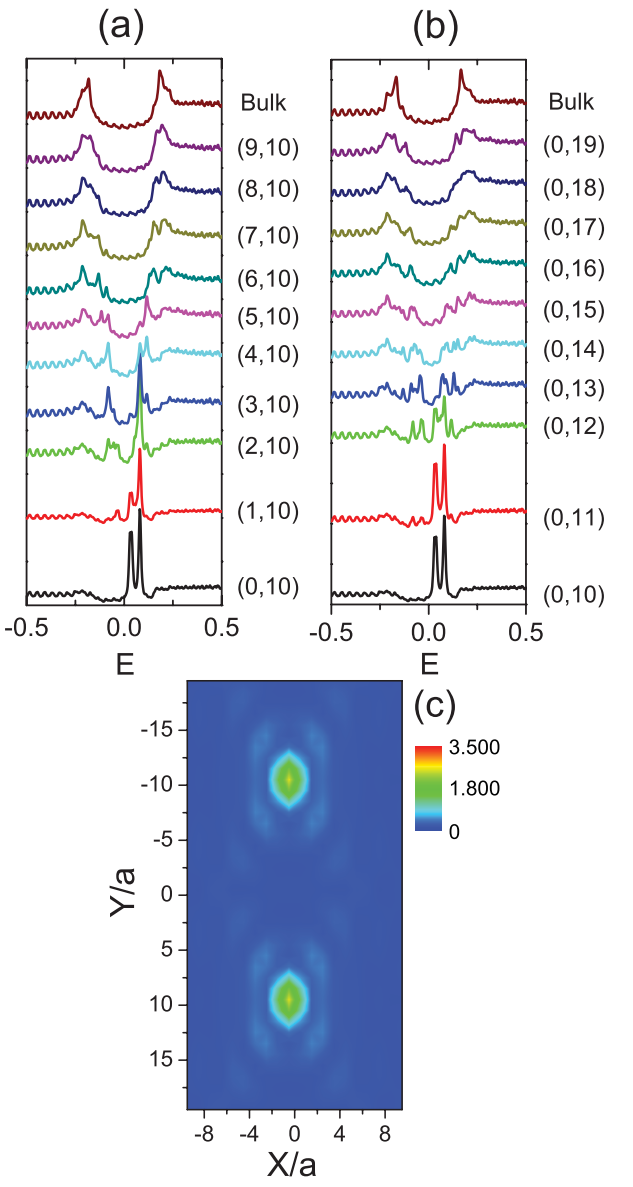

FIG. 7. (Color online) The LDOS vs tunneling energy E at different sites from the vortex core to outside along (a) the x axis (short axis) and (b) the y axis (long axis). The distances of each site from the vortex core take the step of one lattice constant. (c) The spatial LDOS distributions at the vortex core resonant energy $E_{\mathrm{er}} = 0.038$.

which the oscillation period is related to the external magnetic field.[34] At the vortex core [$\vec{r} = (0,10a)$], the coherence peaks at the bulk gap value of Δ_{ch} disappear. Instead, a resonance peak appears at $E_{\mathrm{re}} \approx 0.062$. Away from the vortex core, the resonance peak splits into the particle and hole branches with energies which symmetrically distribute with respect to E_f. As the distance increases, the peak intensities decrease, and the energy separations between the particle and hole branches of peaks increase. As the distance reaches around $6a$, i.e., beyond the coherence length ξ, these peaks merge into the bulk coherence peaks. Figure 5(e) presents the spatial distribution of the LDOS at the vortex core resonance state energy E_{re}, which exhibits the fourfold rotational symmetry. The vortex

core state mainly distributes within one coherence length; thus, it is closer to a bound state rather than a resonance state.

B. The vortex structures with orbital ordering

In this section, we consider the effect of orbital ordering on the vortex lattice states. The band and interaction parameters are the same as in Sec. V A, except that we add the anisotropy term of Eq. (5) with $\delta\varepsilon = 0.2$. Such a term breaks the degeneracy between the d_{xz} and d_{yz} orbitals and reduces the C_4 symmetry down to C_2.

Figures 6(a), 6(b), and 6(c) depict the spatial distributions of the NN $s_{x^2+y^2}$ pairing order parameters Δ_L^{NN} and Δ_T^{NN}, and the NNN $s_{x^2y^2}$ pairing order parameters in a magnetic unit cell, respectively. All of them clearly exhibit the breaking of the fourfold symmetry down to the twofold one. For the dominant NN $s_{x^2+y^2}$ pairings, the coherence lengths along the x and y directions are no longer the same, which can be estimated as $\xi_x \approx 3a$ and $\xi_y \approx 7a$, respectively. From the Fermi surface in Fig. 2(b), in the presence of orbital ordering, the electron pocket in the y direction shrinks, which implies that Cooper pairing superfluid stiffness is weaker along the y direction than in the x direction. This picture agrees with the larger value of ξ_y exhibited in Fig. 6.

Next we turn to study the LDOS patterns for the extended $s_{\pm}$ wave with orbital ordering. In comparison with those without orbital ordering depicted in Fig. 5(c), the LDOS patterns in Figs. 7(a) and 7(b) exhibit significant anisotropy. At the vortex core center, the resonance peak splits into two pieces inside the gap. This feature is similar to the previous studies on the $s_{x^2y^2}$-wave pairing with SDW in iron-based superconductors[34] and the d-wave pairing with antiferromagnetic ordering in cuprates.[48] Away from the vortex center, however, the peaks of the particle and hole branches along short (x) and long (y) axes behave differently. The separation between the particle and hole peaks disperses along the short axis much quicker than along the long axis. The peak intensities along the short axis are stronger than those along the long axis. These features are in good agreement with recent experiment observations.[24] The pronounced anisotropy also is exhibited in the spatial variation of the LDOS at the energy $E_{\mathrm{er}} = 0.038$ where the resonance peak is located, presented in Fig. 7(c). Moreover, with negative $\delta\varepsilon$ which loads particles in d_{xz} prior to d_{yz}, all of the above pictures will have a $\pi/2$ rotation. Therefore, the experimentally observed anisotropy agrees with the picture of orbital ordering.

VI. DISCUSSIONS AND CONCLUSIONS

We have studied a minimal two-orbital model with orbital ordering to interpret the recent STM observations in Ref. 24 including the nodal superconductivity and the anisotropy vortex structure in FeSe superconductors. In considering the absence of magnetic long-range order in FeSe at ambient pressure, orbital ordering provides a natural formalism for anisotropy. The NN s_{x+y^2} wave and the NNN $s_{x^2y^2}$ wave are considered, which generally are mixed. When the NNN pairing dominates, nodal pairing still exists even in the presence of orbital ordering. We further performed the BdG calculation for the vortex tunneling spectra in the presence of orbital ordering, which breaks C_4 rotational symmetry down to C_2 and explicitly induces anisotropic vortex structures.

The microscopic mechanism of the origin of this spontaneous anisotropy remains an open question. It might be related to the strong antiferromagnetic fluctuations. As shown in Refs. 49, 21, and 20, before the onset of the antiferromagnetic long-range order, the spin nematic order with a Z_2 symmetry breaking occurs. This nematic order corresponds to anisotropic spin-spin correlation along the a and b axes, which can in turn induce orbital ordering.

Note added. Near the completion of this manuscript, we learned of the paper by Chowdhury *et al.*,[50] which studied the anisotropic vortex tunneling spectra in Ref. 24 through the Ginzburg-Landau formalism.

ACKNOWLEDGMENTS

C.W. thanks Z. Y. Lu and F. J. Ma for helpful discussions. H.H.H. and C.W. are partly supported by the NBRPC (973 Program) Grants No. 2011CBA00300 and No. 2011CBA00302, Grant No. NSF-DMR-1105945, and the Sloan Research Foundation. C.L.S., X.C., X.C.M., and Q.K.X. are supported by the National Science Foundation and Ministry of Science and Technology of China.

*On leave for the Department of Electrical and Computer Engineering, University of Illinois at Urbana-Champaign, Urbana, Illinois 61801, USA.

[1] Y. Kamihara, T. Watanabe, M. Hirano, and H. Nosono, J. Am. Chem. Soc. **130**, 3296 (2008).
[2] C. de la Cruz *et al.*, Nature (London) **453**, 899 (2008).
[3] T. Hanaguri, S. Nittaka, K. Kuroki, and H. Takagi, Sceince **328**, 474 (2010).
[4] X. Zhang, Y. S. Oh, Y. Liu, L. Yan, K. H. Kim, R. L. Greene, and I. Takeuchi, Phys. Rev. Lett. **102**, 147002 (2009).
[5] H. Ding *et al.*, Europhys. Lett. **83**, 47001 (2008).
[6] K. Seo, B. A. Bernevig, and J. Hu, Phys. Rev. Lett. **101**, 206404 (2008).
[7] M. Daghofer, A. Moreo, J. A. Riera, E. Arrigoni, D. J. Scalapino, and E. Dagotto, Phys. Rev. Lett. **101**, 237004 (2008); A. Moreo, M. Daghofer, J. A. Riera, and E. Dagotto, Phys. Rev. B **79**, 134502 (2009).
[8] F. Wang, H. Zhai, Y. Ran, A. Vishwanath, and D. H. Lee, Phys. Rev. Lett. **102**, 047005 (2009).
[9] V. Cvetkovic and Z. Tesanovic, Europhys. Lett. **85**, 37002 (2009).
[10] V. Cvetkovic and Z. Tesanovic, Phys. Rev. B **80**, 024512 (2009).
[11] M. R. Norman, Physics **1**, 21 (2008).
[12] J. D. Fletcher, A. Serafin, L. Malone, J. G. Analytis, J. H. Chu, A. S. Erickson, I. R. Fisher, and A. Carrington, Phys. Rev. Lett. **102**, 147001 (2009).

[13]C. W. Hicks, T. M. Lippman, M. E. Huber, J. G. Analytis, J. H. Chu, A. S. Erickson, I. R. Fisher, and K. A. Moler, Phys. Rev. Lett. **103**, 127003 (2009).
[14]B. Zeng, G. Mu, H. Q. Luo, T. Xiang, H. Yang, L. Shan, C. Ren, I. I. Mazin, P. C. Dai, and H.-H. Wen, Nat. Commun. **1**, 112 (2010).
[15]I. I. Mazin, D. J. Singh, M. D. Johannes, and M. H. Du, Phys. Rev. Lett. **101**, 057003 (2008).
[16]Z.-J. Yao, J.-X. Li, and Z. D. Wang, New. J. Phys. **11**, 025009 (2009).
[17]F. Wang, H. Zhai, and D.-H. Lee, Phys. Rev. B **81**, 184512 (2010).
[18]F. Wang, H. Zhai, Y. Ran, A. Vishwanath, and D.-H. Lee, Phys. Rev. Lett. **102**, 047005 (2009).
[19]Y. Chen, J. W. Lynn, J. Li, G. Li, G. F. Chen, J. L. Luo, N. L. Wang, P. Dai, C. de la Cruz, and H. A. Mook, Phys. Rev. B **78**, 064515 (2008).
[20]C. Fang, H. Yao, W.-F. Tsai, J. P. Hu, and S. A. Kivelson, Phys. Rev. B **77**, 224509 (2008).
[21]C. Xu, M. Muller, and S. Sachdev, Phys. Rev. B **78**, 020501(R) (2008).
[22]S. Li, C. de la Cruz, Q. Huang, Y. Chen, J. W. Lynn, J. Hu, Y.-L. Huang, F. Hsu, K.-W. Yeh, M.-K. Wu, and P. Dai, Phys. Rev. B **79**, 054503 (2009).
[23]Wei Bao, Y. Qiu, Q. Huang, M. A. Green, P. Zajdel, M. R. Fitzsimmons, M. Zhernenkov, S. Chang, M. Fang, B. Qian, E. K. Vehstedt, J. Yang, H. M. Pham, L. Spinu, and Z. Q. Mao, Phys. Rev. Lett. **102**, 247001 (2009).
[24]C.-L. Song, Y.-L. Wang, P. Cheng, Y.-P. Jiang, W. Li, T. Zhang, Z. Li, K. He, L. Wang, J.-F. Jia, H.-H. Hung, C. Wu, X. Ma, X. Chen, and Q.-K. Xue, Science **332**, 1410 (2011).
[25]J. Knolle, I. Eremin, A. Akbari, and R. Moessner, Phys. Rev. Lett. **104**, 257001 (2010).
[26]S. Medvedev *et al*., Nat. Mater. **8**, 630 (2009).
[27]W. C. Lee and C. Wu, Phys. Rev. B **80**, 104438 (2009).
[28]S. Raghu, A. Paramekanti, E. A. Kim, R. A. Borzi, S. A. Grigera, A. P. Mackenzie, and S. A. Kivelson, Phys. Rev. B **79**, 214402 (2009).
[29]W. C. Lee, D. P. Arovas, and C. Wu, Phys. Rev. B **81**, 184403 (2010).
[30]W. C. Lee and C. Wu, Phys. Rev. Lett. **103**, 176101 (2009).
[31]S. Raghu, X.-L. Qi, C.-X. Liu, D. J. Scalapino, and S.-C. Zhang, Phys. Rev. B **77**, 220503(R) (2008).
[32]W.-F. Tsai, Y.-Y. Zhang, C. Fang, and J. Hu, Phys. Rev. B **80**, 064513 (2009).
[33]T. Zhou, X. Hu, J.-X. Zhu, and C. S. Ting, e-print arXiv:0904.4273.
[34]X. Hu, C. S. Ting, and J.-X. Zhu, Phys. Rev. B **80**, 014523 (2009).
[35]H.-M. Jiang, J. X. Li, and Z. D. Wang, Phys. Rev. B **80**, 134505 (2009).
[36]Y.-Y. Zhang, C. Fang, X. Zhou, K. Seo, W. F. Tsai, B. A. Bernevig, and J. Hu, Phys. Rev. B **80**, 094528 (2009).
[37]S. Lebegue, Phys. Rev. B **75**, 035110 (2007); D. H. Lu, M. Yi, S.-K. Mo, A. S. Erickson, J. Analytis, J.-H. Chu, D. J. Singh, Z. Hussain, T. H. Geballe, I. R. Fisher, and Z.-X. Shen, Nature **455**, 81 (2008).
[38]F. Krüger, S. Kumar, J. Zaanen, and J. van den Brink, Phys. Rev. B **79**, 054504 (2009).
[39]C.-C. Lee, W.-G. Yin, and W. Ku, Phys. Rev. Lett. **103**, 267001 (2009).
[40]W. Lv, J. Wu, and P. Phillips, Phys. Rev. B **80**, 224506 (2009).
[41]C.-C. Chen, J. Maciejko, A. P. Sorini, B. Moritz, R. R. P. Singh, and T. P. Devereaux, Phys. Rev. B **82**, 100504(R) (2010).
[42]W. Lv, F. Krüger, and P. Phillips, Phys. Rev. B **82**, 045125 (2010).
[43]W. Lv and P. Phillips, Phys. Rev. B **84**, 174512 (2011).
[44]Q. Han, J. Phys. Condens. Matter **22**, 035702 (2010).
[45]F. Yang, H. Zhai, F. Wang, and D.-H. Lee, Phys. Rev. B **83**, 134502 (2011).
[46]C.-L. Song, Y.-L. Wang, P. Cheng, Y.-P. Jiang, W. Li, T. Zhang, Z. Li, K. He, L. Wang, J.-F. Jia, H.-H. Hung, C. Wu, X. Ma, X. Chen, and Q.-K. Xue, Supporting Online Material in Science **332**, 1410 (2011).
[47]Y. Gao, H.-X. Huang, C. Chen, C. S. Ting, and W.-P. Su, Phys. Rev. Lett. **106**, 027004 (2011).
[48]J.-X. Zhu and C. S. Ting, Phys. Rev. Lett. **87**, 147002 (2001).
[49]R. M. Fernandes, A. V. Chubukov, J. Knolle, I. Eremin, and J. Schmalian, Phys. Rev. B **85**, 024534 (2012)
[50]D. Chowdhury, E. Berg, and S. Sachdev, Phys. Rev. B **84**, 205113 (2011).